UNIVERSITÄT AUGSBURG
Universitätsbibliothek

OPEN ACCESS
OPUS AUGSBURG

Nonlinear temperature dependency of cell mechanics and consequences for potential filter applications

Simon Valentin Neidinger, Christoph Westerhausen

Angaben zur Veröffentlichung / Publication details:

Neidinger, Simon Valentin, and Christoph Westerhausen. 2026. "Nonlinear temperature dependency of cell mechanics and consequences for potential filter applications." *Acta Biomaterialia* 214: 382–91. https://doi.org/10.1016/j.actbio.2026.03.016.

Nutzungsbedingungen / Terms of use:

CC BY 4.0

Dieses Dokument wird unter folgenden Bedingungen zur Verfügung gestellt: / This document is made available under these conditions:
CC-BY 4.0: Creative Commons: Namensnennung
Weitere Informationen finden Sie unter: / For more information see:
https://creativecommons.org/licenses/by/4.0/deed.de

Acta Biomaterialia 214 (2026) 382–391

Contents lists available at ScienceDirect

Acta Biomaterialia

journal homepage: www.elsevier.com/locate/actbio

Full length article

Nonlinear temperature dependency of cell mechanics and consequences for potential filter applications

Simon Valentin Neidinger [a,b], Christoph Westerhausen [a,b,c,*]

[a] Physiology, Faculty of Medicine, Institute of Theoretical Medicine, University of Augsburg, 86159 Augsburg, Germany
[b] Institute of Physics, University of Augsburg, 86159 Augsburg, Germany
[c] Center for Advanced Analytics and Predictive Sciences, University of Augsburg, 86159 Augsburg, Germany

ARTICLE INFO

Keywords:
Cell mechanics
Atomic force spectroscopy
AFM
Viscoelasticity
Adhesion
Temperature
Cell filter

ABSTRACT

Label-free filter systems are of great interest for extracting circulating tumor cells from patient blood based on their mechanical properties. However, temperature dependence in this field has so far hardly been considered and previous studies do not cover a wider range of temperatures, allowing only limited insight into the correlation with the mechanical properties. Here, we use atomic force spectroscopy applied to single cells to investigate temperature dependence of mechanic cell properties at eight different temperatures between 15 °C and 39 °C. A strong, partly non-linear temperature dependency of the Young's modulus E, pause deformation d_p and maximal adhesion force F_{adh} of silicon nitride to A375 melanoma cells is shown, which occurs independently of the cell size and on the time scale of a few minutes after temperature variation. Here, E, d_p and F_{adh} change by a factor of about 2.2, 1.4 and 2.7 respectively between 17 °C and 37 °C. To test the applicability of the results in the field of filtration, a microfluidic experiment with channels that contain filter structures with decreasing pore sizes is conducted to quantify cell capture size and temperature dependency. As predicted from the non-linear temperature dependent viscoelastic properties, the cells can penetrate to smaller pore sizes at higher temperatures.

Statement of significance: This study systematically measures how melanoma cell mechanics change with temperature, using fine temperature steps across a broad physiological range. We find that stiffness, deformability, and adhesion vary strongly and nonlinearly with temperature, independent of cell size or scan direction. These results were further validated in microfluidic filter experiments, confirming that temperature-controlled changes in mechanical behavior can be exploited for selective cell separation. The comprehensive dataset and experimental approach advance understanding of temperature-dependent cell viscoelasticity and demonstrate its relevance for biomedical filtration technologies. This work introduces a new perspective on using physical cell properties, rather than biochemical labeling, for potential applications in cancer diagnostics and circulating tumor cell isolation.

1. Introduction

Circulating tumor cells (CTC) play an important role in the process of metastasis formation [1]. Filtering these tumor cells label-free from blood for further analysis is still a big challenge that can be addressed using various microfluidic methods such as filters, diagonal ridges or inertial effects that rely on basic physical cell properties such as size, stiffness, viscoelasticity or deformability [2–6]. The use of mechanical parameters for isolation, such as size, is comparatively simple, fast, and inexpensive, and therefore of great interest [7]. In experiments with colorectal cancer cells spiked whole blood, Ribeiro-Samy et al. achieved an isolation efficiency of 70 % while eliminating 99.99 % of the white blood cell (WBC) population [2]. However, the small number of CTC and overlapping mechanical properties of different cell populations in general impede the filtering process considerably [2,3,8–11]. Allard et al. discovered that on average <10 CTC/ml are found in patient samples and that their diameter d can vary over a wide range from $d < 4$ μm to $d > 30$ μm even within a single patient [8]. Coumans et al. note a clear overlap in the cell sizes of WBC and CTC and point out the size difference between CTC and cultured cell lines [11]. Islam et al. recognised considerable similarities between the Young's modulus of WBC and Jurkat leukemia cells [3]. Chen et al. and Islam et al. showed clearly

* Corresponding author.
E-mail address: christoph.westerhausen@uni-a.de (C. Westerhausen).

https://doi.org/10.1016/j.actbio.2026.03.016
Received 4 November 2025; Received in revised form 23 February 2026; Accepted 9 March 2026
Available online 10 March 2026
1742-7061/© 2026 The Author(s). Published by Elsevier Inc. on behalf of Acta Materialia Inc. This is an open access article under the CC BY license (http://creativecommons.org/licenses/by/4.0/).

overlapping elasticities for CTC and WBC, although the different measurement methods of the two studies must be considered here [3,10].

To optimise filter concepts, it is conceivable to take the temperature into account, as this can have an important influence on the mechanical properties of the cells such as the elasticity [9,12–16]. For instance, Sunnerberg et al. showed that the Young's modulus of neurons at 25 °C is 2.1 times the value obtained at 37 °C [13]. Rico et al. were even able to determine a 14-fold decrease between 16 °C and 37 °C with THP-1 monocytic cells [12]. By comparing six cell types, Li et al. showed that a possible temperature dependence of elasticity largely relies on the cell type and that, in principle, constant elasticity or even hardening is possible with increasing temperature [9]. However, temperature has not really been considered in many filter experiments to date [2–5,11]. At the same time, the existing literature usually shows little insight into the correlation between temperature and cell mechanics, as often only a small amount of data points on the temperature scale (for example room temperature and 37 °C) and only a low cell number was measured or completely different methods were used [9,12–14,17].

To address this problem, we perform elasticity measurements using atomic force microscopy (AFM). The investigated A375 melanoma cells are indented with a flat cantilever up to a distinct force. Moreover, the viscoelastic behavior under constant force and the adhesion force between cantilever and cell are extracted at a specific temperature. Here we refer in detail to the measurement method of our previous work, in which we were able to show that the measurement of the overall elasticity of cells in a microfluidic manner is comparable to the method using a cantilever without tip, suggesting transferability of the approach used here [18]. Under these conditions as contact geometry a large sphere is assumed [18]. As this method delivers the desired parameters as global parameters for the whole cell, in contrast to local analysis employing an indenter with tip, and additionally enables cells to be measured multiple times under precise conditions we here stick with this method to allow for application of our results for the field of cell filters [18,19]. Consequently, the question arises as to what extent the information obtained from AFM measurements on potentially temperature-dependent cell mechanics can actually be transferred to filter processes for cells.

The structure of the paper is as follows. First, the temperature dependence of the mechanical cell properties is analyzed in detail and checked for possible further parameter dependencies. Afterwards, as a proof of principle, it is investigated whether these results are applicable to filter systems. To do so, experiments are conducted to determine the pore sizes at which the cells become stuck at different temperatures.

2. Methods

A more detailed explanation of the sections ‘AFM temperature measurements’ and ‘AFM data acquisition and processing’ can be found in the SI.

2.1. Cell culture and sample preparation

The measurements were carried out with A375 human melanoma cells (ATCC CRL-1619) as an exemplary approximation model for CTC. They were cultured at 37 °C and 5 % CO_2 atmosphere in DMEM (BS.FG 0436, Bio&Sell GmbH, Germany, or comparable), supplemented with 10 % FBS (FBS.S 0615, Bio&Sell) and 1 % penicillin-streptomycin (BS.A 2213, Bio&Sell).

2.2. AFM temperature measurements

For the AFM measurements, the cells were seeded onto a cover slip without further coating one to three days prior to the experiment and cultivated in the regular medium. The measurements were carried out using a JPK Nano Wizard I and a BioCell for temperature control (Bruker Nano GmbH, Germany). For the experiment, the cover glass with the cells was carefully rinsed with medium without supplements to remove dead cells and installed in the BioCell. Subsequently, the chamber was filled with medium without supplements to proceed the experiment under aqueous conditions. By omitting the supplements, artefacts especially in determination of the adhesion forces due to the presence of FBS may be prevented.

A triangular cantilever with a nominal spring constant of 30 mN/m from the MLCT-O10 series (Bruker Corporation, Massachusetts, USA) was used as the measuring probe. New cantilever chips or chips cleaned in an oxygen plasma processor (Diener electronic GmbH & Co.KG, Germany) rinsed with PBS phosphate buffer (without Ca & Mg, PBS-1A, Capricorn Scientific, Germany) were utilized. The measuring lever was regularly checked for contamination before and during the experiment. The exact spring constant was calibrated at the beginning of the measurement day using the thermal noise method. To calibrate the sensitivity, a few force curves were recorded on an empty cover glass before the actual measurement.

The measurements were carried out on cells of six different passages at eight different temperature points (15.2°, 17°, 21°, 25°, 29°, 33°, 37°, 39°) with data won from 28, 48, 67, 87, 93, 70, 55 and 35 cells, respectively. The six temperature points in the middle of the temperature range are chosen equidistantly and are completed by the two edge points, whereby the otherwise very small temperature tolerances are slightly higher at the lowest temperature, as this temperature is close to the technical limit. Due to the lower cell numbers at 15.2 °C and 39 °C, these data points are shown but not used for further quantitative analysis.

To analyze the temperature dependence more precisely, for each partial measurement, unless individual circumstances required in rare cases otherwise, five cells were measured three times consecutively (change cell after every force curve, see Fig. 1C), before the temperature was changed, and then the same cells were analyzed again. The mean value per cell and temperature was used for further analysis. The measurement at one temperature itself took about three minutes, and the temperature adjustment to a new temperature value took five to ten minutes. The same five cells were measured at four temperatures per partial measurement (see Fig. 2A). The set of all results of the described partial measurements covers the desired broad temperature interval. In total, 122 cells were analyzed. To avoid time-related artifacts, the starting temperature was kept constant for about 30 min before starting the experiments. Both increasing and decreasing temperature ramps were applied in about half of the measurements, respectively. With regard to cell viability, other experiments conducted under comparable time and temperature conditions yielded values of over 90 % (data not shown).

2.3. AFM data acquisition and processing

Using AFM, we examined the elastic (Young’s) modulus, pause deformation, and adhesion force between cantilever and the cell. For this purpose, force curves were recorded as exemplarily shown in Fig. 1A and 1B The cells were indented at a speed of 1 μm/s and an increasing force of up to $F = 2$ nN with the flat cantilever (approach). After a one-second break at constant force (pause) the cantilever was retracted again at the same speed (retract).

For the determination of the Young’s modulus, we assume that the contact area between a spherical measuring tip and a straight surface is comparable to that of a flat measuring tip and a rounded cell. Previous work by our group confirmed that this approach enables good comparability with microfluidic approaches [18]. The Young's modulus can therefore be determined from the approach curve with a fit model (Fig. 1B, *YM*) provided by JPK Bruker using the variant of the Hertz model for a spherical indenter with a radius of $r = 10$ μm [20]. A detailed assessment of the fit model can be found in the SI. The applied Poisson ratio is $\nu = 0.5$, which is typically used and stands for the assumption of incompressibility of the tested material [21,22]. An upper limit of

around 10 % of the cell height is generally recommended as the maximum penetration depth for the fit to minimize the influence of the substrate [20,23]. However, to allow for a higher number of data points to fit with the Hertz model, we decided on an upper limit for the indentation depth of 1 μm, which is slightly above this limit (data not shown). A comparison to a lower fit height is presented later.

To determine the adhesion, we use the maximum adhesion force (see Fig. 1B, F_{adh}), as this parameter appears to be comparatively robust against fluctuations in the baseline. To classify the viscous behavior, we define the pause deformation. This is the difference between the cantilever tip positions (AFM head height corrected for cantilever bending) at the beginning and end of our one-second pause segment, during which we keep the force constant (Fig. 1A, d_p).

2.4. Microchannel fabrication

Customized microchannels were used for the filter experiments. These were manufactured using soft lithography, following a protocol of our previous work [18,24]. In short, a negative mold is made from a coated silicon wafer, which can then be filled with an elastomer (PDMS, SYLGARD 184 Silicone Elastomer Kit, The Dow Chemical Company, Michigan, USA). After the elastomer has cured, it can be peeled off, the inlets punched out and bonded to a microscope slide using plasma activation. The channel is now located between the glass and the PDMS. A special channel layout (filter board) was developed for the filter experiments (Fig. 3A). This consists of twelve pore walls with progressively smaller pore sizes in the direction of flow. The channel height is approximately 17 μm, which is slightly greater than the cell size. This ensures that there is no relevant overlap of the cells in the z-direction.

2.5. Filter experiments

To account for biological day-to-day variance, two experiments were performed each day, one at a high temperature (approx. 36 °C) and one at a low temperature (approx. 19 °C), each from a separate cell flask. The filter experiments were carried out during five independent measurement days. The respective microchannel was first rinsed with PBS and subsequently with Albumin bovine Fraction V (10 mg/ml in PBS, SERVA Electrophoresis GmbH, Germany). The adherent cells were removed from the culture, rinsed, detached (0.25 % Trypsin, Sigma-Aldrich Chemie GmbH, Germany), checked for viability, and centrifuged (3 min at 200 g). Subsequently the supernatant was removed, and the cell pellet was resuspended in PBS. For the measurement, the cells were diluted in such a way that enough cells flow through the channel in the further run, but the frame rate (one image every 10 s) is sufficient for adequate temporal resolution. This results in roughly 40 cells/min. The flow rate in the experiment was 150 μl/h.

2.6. Statistics

For the statistical analysis we use 95 % confidence intervals, ANOVA tests with Games-Howell Post Hoc Tests, Pearson's correlation coefficient, two-tailed *t*-tests (without assumption of equal variances) and the intraclass correlation (ICC) to examine the effective sample size [25–29]. As an example, we analyze the ICC of the elasticity values based on the force curves of the 55 cells measured at 37 °C. This examines to what extent the spread of the results within a cell compares to the spread between the cells [25]. Based on the derivation from Liljequist et al. [25] and with the restriction that the number of force curves used per cell varies slightly and was therefore averaged, the result is an ICC of 0.80 and thus a comparatively strong clustering within one cell [26]. This is in line with our previous findings [18]. Therefore, as a conservative approach, the number of cells can be used as the sample size [26]. So, for each temperature, the results will be averaged per cell and the mean values of the cells are then used as individual data points for further evaluations such as confidence intervals.

3. Results

3.1. Temperature dependent mechanical properties

First, in Fig. 1D–F the temperature dependence of various mechanical cell parameters is presented. For this, the results from 122 cells out of six different passages, each measured at four temperatures, were combined. Three force-distance curves were recorded for each temperature on each cell. The Young's modulus as a function of temperature shows that the cells become softer with increasing temperature (Fig. 1D). In the range between 21 °C and 33 °C there is an approximately linear decrease, complemented by two plateaus at higher and lower temperatures. Overall, the Young's modulus changes from $E = (653 \pm 313)$ Pa at 17 °C to $E = (301 \pm 191)$ Pa at 37 °C (mean values with standard deviations), and thus by a factor of more than two. The standard deviations (error bars in Fig. 1D–F) are comparatively high, which is due to the biological variation. However, because of the comparatively high number of cells measured [9,12], the 95 % confidence interval (orange lines) already provides a fairly precise estimate. Between the values of 17 °C and 37 °C there is a strongly significant difference with a p-value (*t*-test) of $p < 0.001$. An overview of the p-values and further statistics (ANOVA) can be found in the SI.

As already mentioned in the method section, the penetration depth into the cell used for the fit is certainly open to debate, especially since Li et al. found that the cell height is temperature-dependent and thus also the potential relative penetration depth [9]. This could affect our results. Therefore, in an additional evaluation, we use a penetration depth of only 0.5 μm as the maximum fit limit (figure S2). Such alternative analysis results in lower absolute values ($E = (376 \pm 296)$ Pa at 17 °C or $E = (176 \pm 117)$ Pa at 37 °C), while the qualitative shape of the curve remains very similar. Only the plateau at low temperatures appears to be less pronounced. Due to the similarity to the previous evaluation method, we will remain with the maximum fit limit of 1 μm in the subsequent course.

The pause deformation d_p shows qualitatively the same temperature dependence (inverted parameter, Fig. 1E). The linear behavior is only slightly shifted towards higher temperatures and the difference between the absolute values is smaller. Thus, the pause deformation changes from $d_p = (135 \pm 41)$ nm at 17 °C to $d_p = (183 \pm 65)$ nm at 37 °C. Here too, there are high standard deviations but relatively narrow confidence intervals. The p-value for the comparison of 17 °C and 37 °C is $p < 0.001$.

Alternatively, the viscoelastic properties can be approximated using dedicated fit models. A corresponding analysis can be found in the SI. In short, it can be seen that, depending on the evaluation method, different conclusions can be drawn about the temperature-dependent viscous behavior. The fit applied to the pause segment predicts in particular the temperature dependence of the elastic component, but less so that of the viscous part. Since this model also works with some assumptions and simplifications, we decided to stay closer to the raw data.

Earlier Li et al. showed that the topography of different cell lines changes with temperature and that the cells are smoother at 37 °C than at room temperature [9]. This could increase the effective contact area and result in changes in adhesion energy. Therefore, we also quantified maximal adhesion force between the cells and the cantilever.

The maximum adhesion force shows an almost linearly decreasing trend over the entire temperature range (Fig. 1F). The maximal adhesion force is $F_{adh} = (649 \pm 239)$ pN for $T = 17$ °C and $F_{adh} = (244 \pm 81)$ pN for $T = 37$ °C. This results in a factor of 2.7. The band of the 95 % confidence interval is even narrower than for elasticity or pause deformation. The p-value for testing F_{adh} for $T = 17$ °C and $T = 37$ °C is $p < 0.001$.

To exclude artifacts, next, we rule out correlations with other measurement parameters. First, we correlate the mechanical properties with the cell size as this could also influence the results [30].

To do so, we divide the measured cells into four quartiles according to size. For elasticity, viscosity and adhesion, all quartiles show

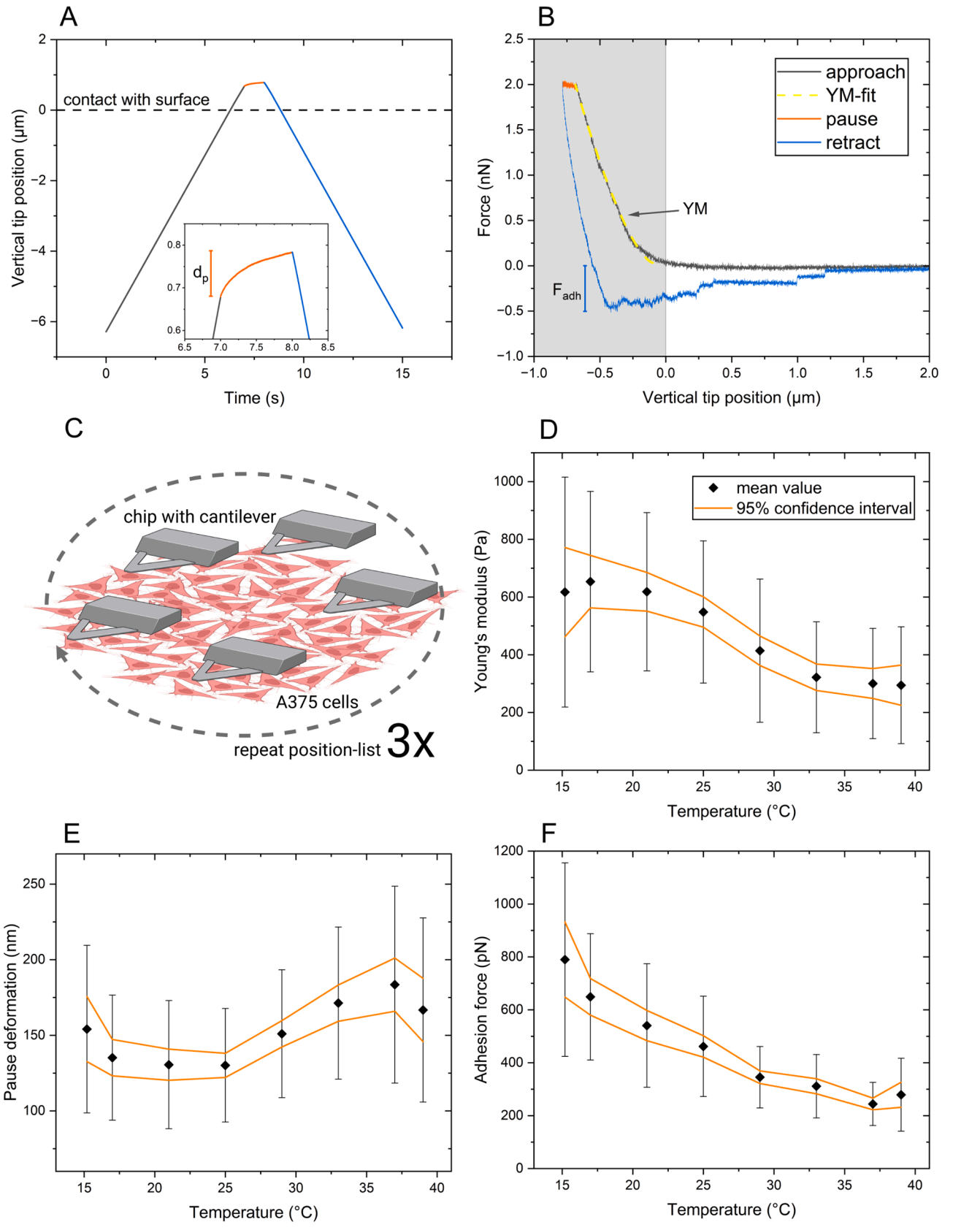

(caption on next page)

Fig. 1. Panel A and B illustrate an exemplary AFM measurement curve with two different representations: Vertical tip position vs. time (A) and force vs. vertical tip position (B). The first curve shows the time profile, the second one the standard force-indentation. The black part of the line represents the approach, the orange part the pause segment and the blue one the retraction. d_p indicates the pause deformation, F_{adh} the maximum adhesion force and YM the curve segment where the Young's modulus fit (yellow) is done. The fit range is marked in grey. Panel C illustrates the measurement procedure (Created in BioRender. Neidinger, S. (2026) https://BioRender.com/2cw8a90). About five cells were measured consecutively three times in one set (change cell after every force curve) before the temperature was adjusted. In one partial measurement, four different temperatures were applied on the same cells. Panel D shows the Young's modulus E, E the pause deformation d_p and F the maximal adhesion force F_{adh}. The points indicate the mean values, the error bars mark the standard deviation and the orange lines the 95 % confidence interval. Each parameter shows a remarkable temperature dependency. Especially for the Young's modulus and the pause deformation d_p the curve differs considerably from a linear trend. The corresponding histograms can be found in Figure S5 in the SI. A total of 122 cells were measured at four temperatures each. Details on the measurement procedure and evaluation can be found in the methods section.

comparable slopes (see figure S3). Only the second quartile is slightly flatter for elasticity and viscosity. We therefore exclude this parameter as a noteworthy influencing factor for the overall temperature dependence.

3.2. Influence of time and measurement direction

In a further step, we check whether our measurement procedure as shown in Fig. 2A influences the results, i.e., whether the direction of the temperature adaptation is important.

As shown in Fig. 2B the Young's modulus in the downscan has a slightly lower temperature dependence. The pause deformation shows a slight offset over large parts of the temperature scale (Fig. 2C). But, in both cases the 95 % confidence intervals still overlap clearly and especially the shape of the up- and downscans is pretty similar. Quantifying adhesion forces both measurement directions show almost identical behavior (Fig. 2D).

Thus, as there no artefacts have been observed, we assume sufficient

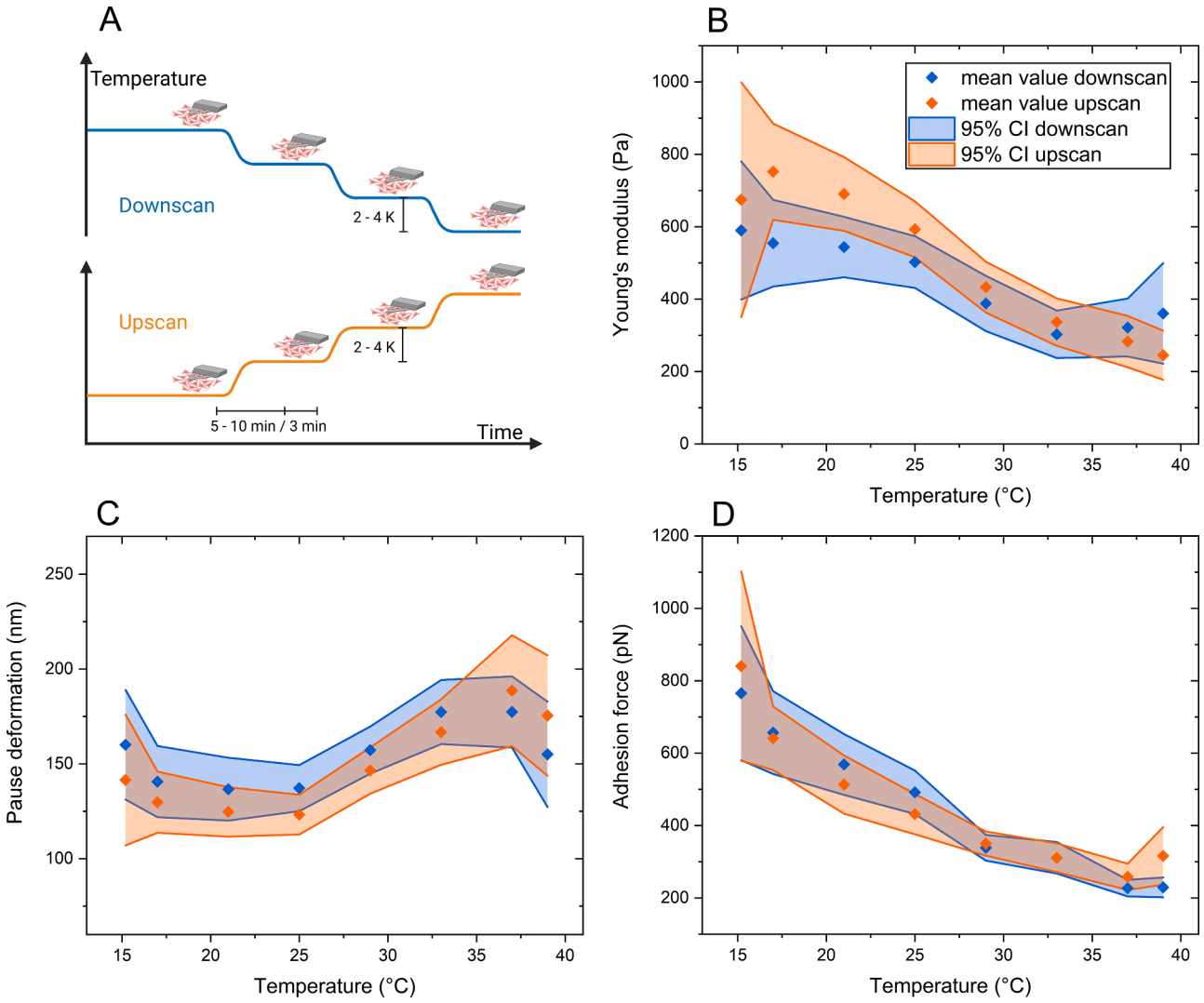

Fig. 2. A illustrates the used temperature profiles: Downscan and upscan (Created in BioRender. Neidinger, S. (2026) https://BioRender.com/xg7p3sh). Each part of a measurement at a distinct temperature and on around five different cells took about three minutes. The time for the adjustment of the temperature took five to ten minutes, depending on multiple aspects. Temperature steps amounted to $\boldsymbol{\Delta T} = 4$ K, except at the smallest and highest temperature ($\boldsymbol{\Delta T} = 2$ K). The other panels show the results for up- (orange) and downscans (blue) separately. Panel B shows the Young's modulus E, C the pause deformation d_p and D the maximal adhesion force F_{adh}. The points indicate the mean values and the colored bands the 95 % confidence interval. For all three parameters the trend of up- and downscan is comparable and the confidence intervals overlap strongly which indicates no considerable differences.

equilibration time for the cells to adapt to the temperature change. Summing up, the applied measurement procedure appears to be robust to other factors underlining the significance of the extracted temperature dependence.

3.3. Applicability of viscoelastic properties obtained employing AFM to filter measurements

Next, the question is addressed whether the results of the AFM measurements can be transferred to filter applications. For this purpose, we measured the average pore size at which the cells get stuck at the two different temperatures (36 °C vs. 19 °C). These temperatures are the limits of what is technically feasible in our design and, with respect to viscoelastic properties, already result in mechanical behavior in the respective plateaus. Since decreasing pore size requires increasingly higher pressure to push the cells through the pores, it can be assumed that the cells get stuck at a distinct size [31]. However, since the pressure on the cells increases as the number of pores blocked by cells increases, the average pore size is examined taking into account the total number of blocked pores (Fig. 3B) [32,33]. To avoid artifacts caused by debris or aggregates, the two edge pore sizes (4.2 μm and 21.1 μm) are excluded from the evaluation.

The average values for the two temperatures show that at higher temperatures the cells tend to penetrate towards smaller pores. Even when considered individually, four of the five measurement days (transparent curves) delivered the same tendency. In the remaining case, a small cell subpopulation with different mechanical properties presumably caused a slight shift in the results.

To address the question of whether the observed effect is actually due to cell mechanics and not size, the cell size of several cells at the channel entrance was quantified. The results show no reduction in cell size for cells at higher temperatures, either on average or in terms of median size (figure S6).

In addition, especially on two of the measurement days, the effect was evident that at 19 °C, one pore wall had to be relatively crowded before the next one was occupied, whereas at 36 °C, the pore walls tended to be occupied simultaneously (Fig. 4). This is shown by the slope of the left flank of the curves (arrows), which represent specific evaluation points in time. An overview of all measurement days can be found in the SI (figure S4). The results from the filter experiments therefore suggest that the findings from the AFM measurements on viscoelasticity can also be transferred and used for the design of future filter applications.

4. Discussion

Following the results of Marcotti et al., we measured a total of 122 cells for our AFM experiments in order to minimize variability in the results and increase reliability [34]. Yang et al. observed significant cellular changes in terms of traction stresses and focal adhesion area when substrate stiffness was continuously altered [35]. Based on this sensitivity to environmental conditions (and environmental hardness), we concluded that as few measurements as possible should be taken per cell in order to avoid any possible impairment due to force loading. Therefore, only three curves were recorded per temperature and cell. The use of the Hertz model with a flat tip and the assumption of a round geometry certainly represents a significant simplification of the actual setup and neglects the viscoelastic behavior of the cell [19]. Due to its validated agreement to microfluidic methods of analyzing elasticity, this simplification was chosen with a view toward the further goal of filtration, allowing the same cells to be measured at multiple temperatures [18]. A more detailed assessment of the evaluation method can be found in the SI. With regard to elasticity and pause deformation, there is a strong temperature dependence, which is particularly non-linear over the whole range and shows plateau-like limit values at high and low temperatures.

The Young's modulus shows a decrease by a factor of 2.2 with increasing temperature from 17 °C to 37 °C. The difference is thus considerably smaller than that observed by Rico et al., who found a factor of 14 for THP-1 cells between 16 °C and 37 °C, albeit with a different AFM setup [12]. Sunnerberg et al., on the other hand, obtained a factor of 2.1 between 25 °C and 37 °C for cortical neurons in AFM measurements with spherical contact geometry, which is very close to our data [13]. Yang et al. used optofluidic microchips to study the deformability of A375 MC2 cells at different temperatures [17]. Since this study does not quantify YM, a direct comparability in terms of absolute values is severely limited, although qualitative similarities can be seen with regard to the temperature dependence of cell deformation

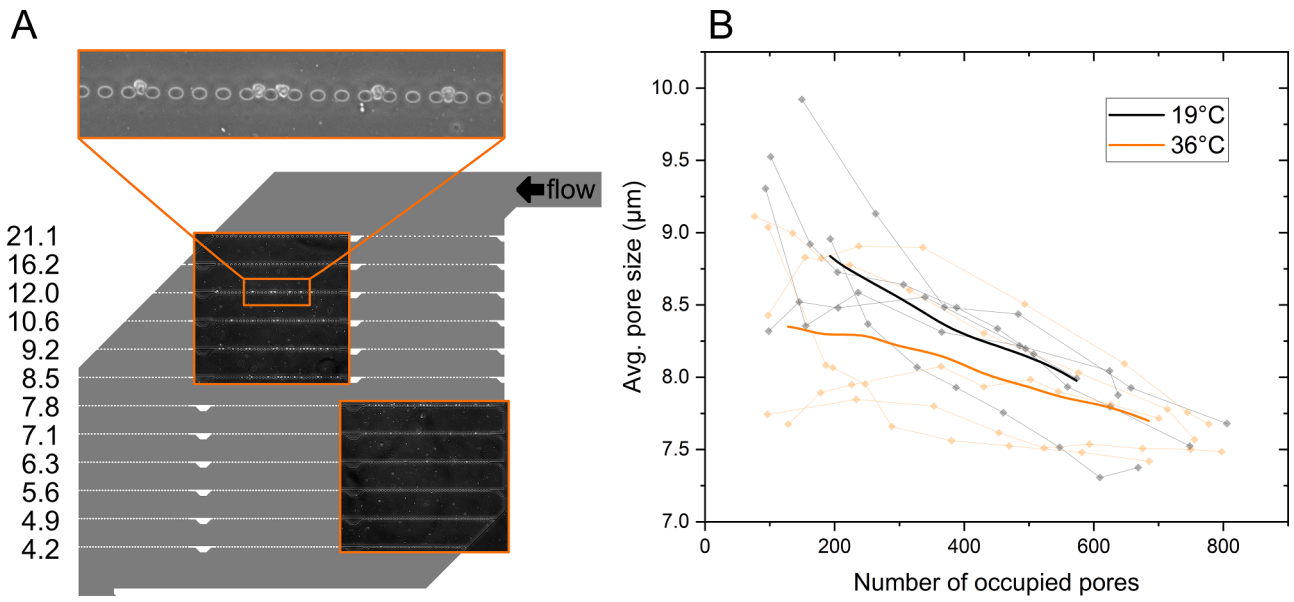

Fig. 3. The filter board in Panel A consists of 12 consecutive pore walls, with decreasing pore width in the direction of flow. The numbers on the left indicate the nominal pore size in μm. The orange overlays show example images from an experiment. Panel B illustrates the average size of occupied pores versus the total number of occupied pores. The light curves show the individual measurements, while the bold curves show the mean value. It is apparent that at higher temperatures, the cells can penetrate to smaller pores.

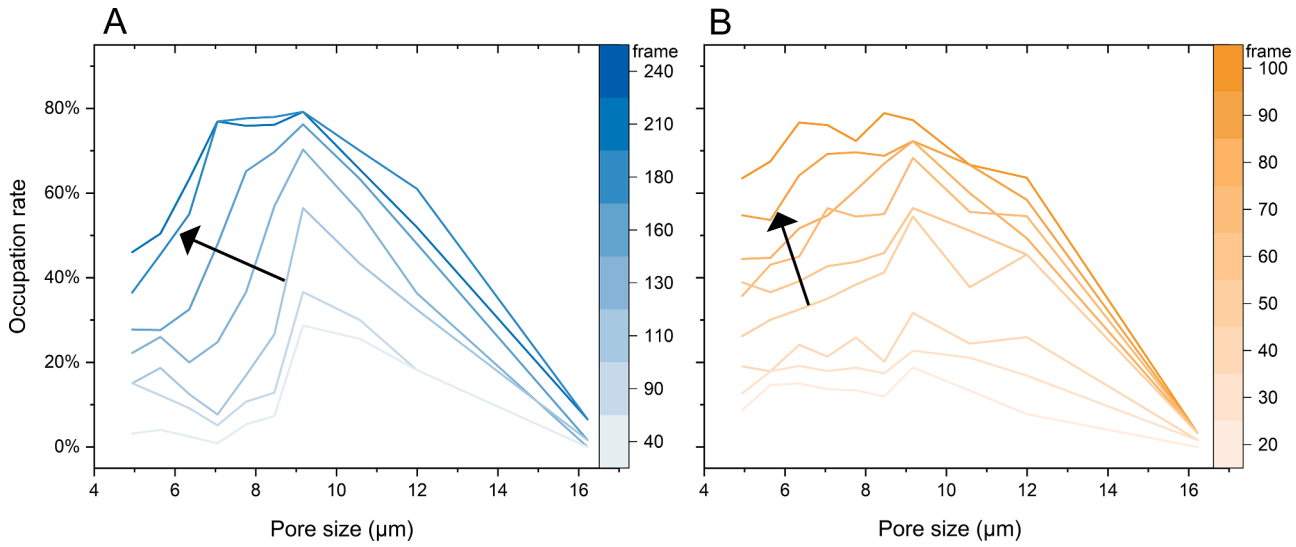

Fig. 4. At low (A) and high (B) temperatures, different dynamics can be observed when looking at the occupancy of the pores per pore size. Each curve represents a specific point in time during the experiment, with the direction of the arrow also indicating the time course. While at 19 °C the pore walls tended to be occupied in sequence, at 36 °C it can be seen that the smaller pore sizes are more likely to be filled simultaneously. Graph shows results from one measurement day and includes a total number of $N = 637$ and $N = 700$ cells for A and B respectively.

[17]. Li et al. were furthermore able to show that the change in elasticity strongly depends on the cell line, for example Jurkat cells became softer with increasing temperature, whereas HeLa cells became harder or white blood cells showed hardly any change [9]. Therefore, the data we measured seem plausible and especially with the combination of the latter mentioned result suggest that the filtering efficiency to catch CTCs in white blood cells should be optimizable by choosing the temperature with the highest spread of the elasticity of both cell types.

The pause deformation in our AFM measurements shows an increase by a factor of 1.4 between 17 °C and 37 °C and can therefore be understood as a decrease in viscosity. Overall, our evaluations for elastic and viscous behavior seem to show a moderate correlation. This might be also a consequence of applying coherent analysis methods. The correlation is also indicated by a Pearson's r value of $r = -0.494$ (conditioned on the temperature).

However, with a view to other publications that analyze the viscoelastic properties our results need to be further classified. Interestingly, Semenov et al. showed with fluorescence anisotropy decay curves, that the microviscosity of the cell membrane of red blood cells decreases with increasing temperature and generally appears to have a comparable temperature behavior to our data for whole cells [36]. Evans and Yeung used micropipette aspiration to examine the viscosity of granulocytes and found a decrease by a factor of approximately 2 when the temperature was elevated from 23 °C to 37 °C [37]. Simon et al. postulated on the other hand by varying the AFM loading speed that the soma of neurons does not show viscous behavior, but the pericellular brush does to some extend [38]. This observation is a strong deviation from our data, which indicate viscous behavior even at a comparatively high penetration depth of around 1 μm. In their work, Sunyer et al. and Kießling et al. found higher elasticity and lower viscosity with increasing temperature [15,16]. However, it should not be forgotten that the temperature-dependent cell mechanical properties are highly dependent on the cell line [9]. Kießling et al. pointed out the possibility that a drastic decrease in viscosity could superimpose an increase in elasticity and that higher deformability could be understood as a lower elastic modulus, although they attributed increased deformability itself more to a lower viscosity [16]. This suggests that the common use of the Hertz model for elasticity analysis, with its basic assumptions, may be compromised by the viscous influence of the cell and therefore falls short [19,20]. However, the decrease in viscosity with increasing temperature found by Sunyer et al. and Kießling et al. is in line with our pause deformation results, as we observed a larger deformation with increasing temperature and thus a more fluid behavior of the cells [15,16]. On the other hand, the evaluation of viscous creep using a fit to the pause segment of the AFM curve shows fundamentally viscoelastic behavior but attributes the temperature dependence mainly to the elastic component (see SI). However, it should be noted that the used fit model also involved relevant assumptions and simplifications. In terms of filter applications and the squeezing through pore walls, it seems more appropriate to use the raw data and consider the full deformation.

Despite all the points of criticism, it should be noted that regardless of the assignment to viscous or elastic behavior, our data shows a strong and finely resolved temperature dependence of the mechanical properties. In combination with the report of Li et al. the option of exploiting a comparatively temperature-stable mechanical behavior of white blood cells compared to strong temperature dependence of the mechanical behavior of our melanoma cell line seems promising [9].

The next mechanical parameter we quantified here, the adhesion of flat silicon nitride cantilevers to melanoma cells, is important, for example, in the context of endocytosis-like nanoparticle uptake [39]. Between 17 °C and 37 °C, our measurements show that the maximum adhesion force decreases by a factor of 2.7 with a comparatively linear trend. Only at high temperatures a slight flattening of the curve can be seen. However, literature research gives a mixed picture. Sagvolden et al. were able to show for human cervical carcinoma cells that at higher temperatures greater forces are sometimes necessary to detach adherent cells from protein coated substrates [40]. Ueda et al. showed that as temperature increases, the number of attached cells increases [41]. Baier et al. also found an increase in the necessary detachment work of mammalian red blood cells with increasing temperature and justified this with an increase in the contact area between the measuring tip and sample [42,43]. The contact area, in turn, is closely related to the elasticity of the cell [43]. Furthermore, Li et al. demonstrated that Hela cells become smoother at higher temperatures which in turn would mean more contact area and thus potentially more adhesion [9,43]. At first glance, this contradicts our results because at low temperatures we measure a high Young's modulus and thus a low penetration depth with a consequently smaller contact area but at the same time also the maximum of adhesion force. But with our cantilever geometry, the contact area is likely to correlate less strongly with the penetration depth than when using sharp tips. Furthermore, we focus on the maximum adhesion force and not the detachment work. Rico et al. showed as well,

that the work of detachment increases with increasing temperature, but the tether force and rupture force of the LFA-1/ICAM-1 complex is significantly higher at low temperatures as well as the adhesion force per perimeter (slightly insignificant) [12]. This seems more compatible with our results and suggests potential differences in the consideration of energies or forces. With regard to the explanation, they mention not only a possible direct temperature effect but also the possibility that the result could be caused by reduced stiffness and thus a reduced loading rate of the retraction [12], which would also be conceivable in our case and could be regarded as a measurement artifact or, with respect to the filtration or absorption of particles, as an actual component to be considered. However, due to different setups, the results are still difficult to compare and the reason for the differences can only be speculated upon. The extent to which, for example, non-specific bonds or certain proteins are significant for our adhesion results cannot be reliably determined based on the setup and also exceeds the scope of this manuscript.

To explore the sensitivity of the reported results to the analysis of the force curves, in a next step, we examined to what extent the mechanical parameters change if the fit range is varied. Moreover, we check for a possible correlation of the quantities with cell size and temporal effects.

First, we reduced the maximum penetration depth for the fit from 1 μm to 0.5 μm in order to avoid a possible substrate influence [20,23]. The aforementioned influence of the substrate becomes even more significant in light of the fact that Li et al. were able to show with Hela cells that cell height can be greater at higher temperatures [9]. To rule out the possibility that the lower Young's modulus at higher temperatures is due to the substrate having less influence as a result of a potentially larger cell height, the reduced fit range is considered. This only affects the obtained Young's modulus but not the measured adhesion force and viscous relaxation. While the absolute values of the Young's modulus in that case are about half as high as for the first analysis, the general shape of the curve is conserved (see figure S2). This is qualitatively consistent with the work of Dokukin et al. dealing with a cell brush but also opens up the question on the extent to which the elastic deformation of the cell body is actually measured in each case [44]. It should be noted that the absolute values are therefore dependent on the overall conditions and can only be interpreted in context. For the reasons mentioned earlier, we consider it unlikely that the temperature dependence is significantly overlaid by the cell height. Nevertheless, it would be advisable to use a standardized relative cell height for indentation, for example, with a view to future measurements or better comparability with other publications. As for potential filter applications the elasticity for stronger deformations seems more relevant and suitable, we chose a maximal penetration depth of 1 μm to report the Young's modulus $E(T)$.

In a next step, we investigated whether there is a correlation between cell size and mechanical properties that overlaps the temperature effect. No noteworthy connection could be detected here (figure S3), which is consistent with the results of Fläschner et al., who also found no correlation between viscoelastic properties and cell size in rounded HeLa cells [45]. Moreover, we checked whether the measurement direction plays a role for the obtained quantities. The adhesion forces do not differ notably between upscans and downscans (see Fig. 2). There were also only small deviations between the two measurement directions for Young's modulus and the pause deformation, where the 95 % confidence intervals always clearly overlap, and especially the qualitative curve remains mostly the same. Considering the comparatively short acclimatization phases between the individual temperature points and the consistent absolute values, the cells appear to react quickly to their ambient temperature. Since several measurements with different ramp directions were often carried out on a single cover slip for a different set of cells, we also conclude that the adaptation of the mechanical cell properties to a new temperature is a comparatively reversible process as no major differences were detectable over time (data not shown). These findings are consistent with results from the literature. Kießling et al. showed that temperature instantaneously changes the deformability of cells in suspension [16]. However, they also found that on short time scales (seconds) only the viscous component is influenced, whereas after longer adjustments (minutes) the elastic component also reacts [16]. Using measurements on individual neurons, Spedden et al. were able to show that there is a high degree of reversibility in elasticity [14].

Summing up these checks for potential artifacts we found no superimposed correlations or dependencies in our measurements and thus the method seems therefore well suited to investigate the temperature dependence of the mechanical cell properties, especially of the here studied A375 cells but potentially also other cell types.

With regard to filter applications, to the best of our knowledge, we have not yet found any comparable work that takes temperature into account as a parameter in filtering in this way. Only Sarioglu et al., for example, tested a temperature change for the release of cells from the channel [46]. Due to the highly customized setup, we are reluctant to give exact numerical values, but it appears rather clear from a qualitative point of view that at lower temperatures, the A375 cells get stuck in larger pores (Fig. 3B) and that this effect is most likely due to the viscoelastic behavior of the cells. This is suggested by the evidence from the size measurements and the dynamics of pore occupation. With regard to the literature, Yang et al. also did not observe any significant temperature-dependent change in size in A375 MC2 cells, but noted that at higher temperatures, in addition to greater deformability of the cells, a higher pressure was required to push cells through a single constriction [17]. At first glance, this contradicts our results. Yang et al. and Martinez Vazquez et al. refer to the increased contact area between the channel walls and the cell, which results from the increased deformability and leads to more friction [17,47]. However, we assume that the pore geometry we chose is considerably less susceptible to this effect, as the pores are designed more like funnels and less like wall recesses [17,47]. With regard to the desired application of CTC filtering, our results represent a certain simplification, as only tumor cells in PBS without other blood components and only two temperature points were analyzed. For a more precise temperature dependence of the filter characteristics, further measurements with finer temperature gradation would be of interest. Nevertheless, a general temperature pattern was clearly discernible. However, in view of our measurements, future experiments, and the results of other groups, which suggest, for example, comparatively temperature-stable mechanical properties of WBCs, the promising question arises as to whether, by choosing the appropriate temperature, a kind of sweet spot could be found where the differentiation of cells based on their mechanical properties and thus the filtering works better than, for example, at room temperature [9,11]. To this end, it would be useful to expand existing filter experiments with whole blood to include temperature as an additional parameter [2].

5. Conclusion

With the study presented here we were able to set new standards with fine resolution and, for AFM studies, a large number of cells on a broad temperature range. The temperature dependence reveals an approximately linear trend for the mechanical properties, complemented by a plateau-like behavior at the edges in the range of 17 °C and 37 °C. In combination with filter experiments, it seems promising, e.g., to optimize the filtering of circulating tumor cells from blood samples based on the different temperature behavior of different cells [9].

Data availability

Data is available on request.

Funding sources

SVN and CW would like to acknowledge support by the Center for NanoScience (CeNS) and the Hanns-Seidel-Stiftung. CW would like to acknowledge funding by the DFG (508235635).

Acknowledgements

We thank Achim Wixforth for fruitful discussions.

CRediT authorship contribution statement

Simon Valentin Neidinger: Writing – review & editing, Writing – original draft, Visualization, Validation, Methodology, Investigation, Funding acquisition, Formal analysis, Data curation, Conceptualization. **Christoph Westerhausen:** Writing – review & editing, Writing – original draft, Visualization, Validation, Supervision, Resources, Project administration, Methodology, Funding acquisition, Conceptualization.

Declaration of competing interest

The authors declare that they have no known competing financial interests or personal relationships that could have appeared to influence the work reported in this paper.

Supplementary materials

Supplementary material associated with this article can be found, in the online version, at doi:10.1016/j.actbio.2026.03.016.

References

[1] R.L. Anderson, T. Balasas, J. Callaghan, R.C. Coombes, J. Evans, J.A. Hall, S. Kinrade, D. Jones, P.S. Jones, R. Jones, J.F. Marshall, M. Panico, J.A. Shaw, P. S. Steeg, M. Sullivan, W. Tong, A.D. Westwell, J.W.A Ritchie, A framework for the development of effective anti-metastatic agents, Nat. Rev. Clin. Oncol. 16 (3) (2019) 185–204, https://doi.org/10.1038/s41571-018-0134-8.

[2] S. Ribeiro-Samy, M.I. Oliveira, T. Pereira-Veiga, L. Muinelo-Romay, S. Carvalho, J. Gaspar, P.P. Freitas, R. López-López, C. Costa, L. Diéguez, Fast and efficient microfluidic cell filter for isolation of circulating tumor cells from unprocessed whole blood of colorectal cancer patients, Sci. Rep. 9 (1) (2019), https://doi.org/10.1038/s41598-019-44401-1.

[3] M. Islam, A. Raj, B. McFarland, H.M. Brink, J. Ciciliano, M. Fay, D.R. Myers, C. Flowers, E.K. Waller, W. Lam, A. Alexeev, T. Sulchek, Stiffness based enrichment of leukemia cells using microfluidics, APL. Bioeng. 4 (3) (2020), https://doi.org/10.1063/1.5143436.

[4] G. Wang, K. Crawford, C. Turbyfield, W. Lam, A. Alexeev, T. Sulchek, Microfluidic cellular enrichment and separation through differences in viscoelastic deformation, Lab. Chip. 15 (2) (2015) 532–540, https://doi.org/10.1039/c4lc01150c.

[5] M.G. Lee, J.H. Shin, C.Y. Bae, S. Choi, J.K. Park, Label-free cancer cell separation from human whole blood using inertial microfluidics at low shear stress, Anal. Chem. 85 (13) (2013) 6213–6218, https://doi.org/10.1021/ac4006149.

[6] X.L. Zhang, P.P. Xie, K.T. Zhang, W. Zhang, Circulating tumour cell isolation, analysis and clinical application, Cell. Oncol. 46 (3) (2023) 533–544, https://doi.org/10.1007/s13402-023-00774-0.

[7] G. Vona, A. Sabile, M. Louha, V. Sitruk, S. Romana, K. Schütze, F. Capron, D. Franco, M. Pazzagli, M. Vekemans, B. Lacour, C. Bréchot, P. Paterlini-Bréchot, Isolation by size of epithelial tumor cells: a new method for the immunomorphological and molecular characterization of circulating tumor cells, Am. J. Pathol. 156 (1) (2000) 57–63, https://doi.org/10.1016/S0002-9440(10)64706-2.

[8] W.J. Allard, J. Matera, M.C. Miller, M. Repollet, M.C. Connelly, C. Rao, A.G. J. Tibbe, J.W. Uhr, L.W.M.M Terstappen, Tumor cells circulate in the peripheral blood of all major carcinomas but not in healthy subjects or patients with nonmalignant diseases, Clin. Cancer Res. 10 (20) (2004) 6897–6904, https://doi.org/10.1158/1078-0432.CCR-04-0378.

[9] M. Li, L.Q. Liu, N. Xi, Y.C. Wang, X.B. Xiao, W.J. Zhang, Effects of temperature and cellular interactions on the mechanics and morphology of human cancer cells investigated by atomic force microscopy, Sci. China Life Sci. 58 (9) (2015) 889–901, https://doi.org/10.1007/s11427-015-4914-4.

[10] C.L. Chen, D. Mahalingam, P. Osmulski, R.R. Jadhav, C.M. Wang, R.J. Leach, T. C. Chang, S.D. Weitman, A.P. Kumar, L. Sun, M.E. Gaczynska, I.M. Thompson, T.H. M. Huang, Single-cell analysis of circulating tumor cells identifies cumulative expression patterns of EMT-related genes in metastatic prostate cancer, Prostate 73 (8) (2013) 813–826, https://doi.org/10.1002/pros.22625.

[11] F.A.W. Coumans, G. van Dalum, M. Beck, L.W.M.M. Terstappen, Filter characteristics influencing circulating tumor cell enrichment from whole blood, PLoS. One 8 (4) (2013), https://doi.org/10.1371/journal.pone.0061770.

[12] F. Rico, C. Chu, M.H. Abdulreda, Y. Qin, V.T. Moy, Temperature modulation of integrin-mediated cell adhesion, Biophys. J. 99 (5) (2010) 1387–1396, https://doi.org/10.1016/j.bpj.2010.06.037.

[13] J.P. Sunnerberg, P. Moore, E. Spedden, D.L. Kaplan, C. Staii, Variations of elastic modulus and cell volume with temperature for cortical neurons, Langmuir 35 (33) (2019) 10965–10976, https://doi.org/10.1021/acs.langmuir.9b01651.

[14] E. Spedden, D.L. Kaplan, C. Staii, Temperature response of the neuronal cytoskeleton mapped via atomic force and fluorescence microscopy, Phys. Biol. 10 (5) (2013), https://doi.org/10.1088/1478-3975/10/5/056002.

[15] R. Sunyer, X. Trepat, J.J. Fredberg, R. Farré, D. Navajas, The temperature dependence of cell mechanics measured by atomic force microscopy, Phys. Biol. 6 (2) (2009), https://doi.org/10.1088/1478-3975/6/2/025009.

[16] T.R. Kießling, R. Stange, J.A. Käs, A.W. Fritsch, Thermorheology of living cells - impact of temperature variations on cell mechanics, New J. Phys. 15 (4) (2013), https://doi.org/10.1088/1367-2630/15/4/045026.

[17] T. Yang, G. Nava, P. Minzioni, M. Veglione, F. Bragheri, F.D. Lelii, R.M. Vazquez, R. Osellame, I. Cristiani, Investigation of temperature effect on cell mechanics by optofluidic microchips, Biomed. Opt. Express. 6 (8) (2015) 2991–2996, https://doi.org/10.1364/BOE.6.002991.

[18] A.M. Jötten, S.V. Neidinger, J.K. Tietze, J. Welzel, C. Westerhausen, Dynamic effective elasticity of melanoma cells under shear and elongational flow confirms estimation from force spectroscopy, Biophysica 1 (4) (2021) 445–457, https://doi.org/10.3390/biophysica1040032.

[19] M. Krieg, G. Fläschner, D. Alsteens, B.M. Gaub, W.H. Roos, G.J.L. Wuite, H.E. Gaub, C. Gerber, Y.F. Dufrêne, D.J. Müller, Atomic force microscopy-based mechanobiology, Nat. Rev. Phys. 1 (1) (2019) 41–57, https://doi.org/10.1038/s42254-018-0001-7.

[20] JPK DP Data Processing Software Manual Version 5.0. (2015).

[21] E. A-Hassan, W.F. Heinz, M.D. Antonik, N.P. D'Costa, S. Nageswaran, C. A. Schoenenberger, J.H Hoh, Relative microelastic mapping of living cells by atomic force microscopy, Biophys. J. 74 (3) (1998) 1564–1578, https://doi.org/10.1016/S0006-3495(98)77868-3.

[22] L.M. Rebelo, J.S. de Sousa, J. Mendes Filho, M. Radmacher, Comparison of the viscoelastic properties of cells from different kidney cancer phenotypes measured with atomic force microscopy, Nanotechnology 24 (5) (2013), https://doi.org/10.1088/0957-4484/24/5/055102.

[23] A.B. Mathur, A.M. Collinsworth, W.M. Reichert, W.E. Kraus, G.A. Truskey, Endothelial, cardiac muscle and skeletal muscle exhibit different viscous and elastic properties as determined by atomic force microscopy, J. Biomech. 34 (12) (2001) 1545–1553, https://doi.org/10.1016/S0021-9290(01)00149-X.

[24] Y. Xia, G.M. Whitesides, Soft lithography, Angew. Chem. Int. Ed. 37 (5) (1998) 550–575, https://doi.org/10.1002/(SICI)1521-3773(19980316)37.

[25] D. Liljequist, B. Elfving, K.S. Roaldsen, Intraclass correlation – A discussion and demonstration of basic features, PLoS. One 14 (7) (2019), https://doi.org/10.1371/journal.pone.0219854.

[26] M.B. Sikkel, D.P. Francis, J. Howard, F. Gordon, C. Rowlands, N.S. Peters, A. R. Lyon, S.E. Harding, K.T. Macleod, Hierarchical statistical techniques are necessary to draw reliable conclusions from analysis of isolated cardiomyocyte studies, Cardiovasc. Res. 113 (14) (2017) 1743–1752, https://doi.org/10.1093/cvr/cvx151.

[27] D.A. Eisner, Pseudoreplication in physiology: more means less. Journal of General Physiology (Vol. 153, Issue 2), Rockefeller University Press, 2021, https://doi.org/10.1085/JGP.202012826.

[28] Goss-Sampson, M.A. (2024) Statistical Analysis in Jasp – a guide for students.

[29] A.P. Field, Discovering Statistics using SPSS, SAGE Publications, 2009.

[30] K. Mendová, M. Otáhal, M. Drab, M. Daniel, Size matters: rethinking Hertz model interpretation for cell mechanics using AFM, Int. J. Mol. Sci. 25 (13) (2024) 7186, https://doi.org/10.3390/ijms25137186.

[31] Z. Zhang, J. Xu, B. Hong, X. Chen, The effects of 3D channel geometry on CTC passing pressure–towards deformability-based cancer cell separation, Lab. Chip. 14 (14) (2014) 2576–2584, https://doi.org/10.1039/C4LC00301B.

[32] S. Zheng, H.K. Lin, B. Lu, A. Williams, R. Datar, R.J. Cote, Y.C. Tai, 3D microfilter device for viable circulating tumor cell (CTC) enrichment from blood, Biomed. Microdevices 13 (1) (2011) 203–213, https://doi.org/10.1007/s10544-010-9485-3.

[33] F.A.W. Coumans, G. Van Dalum, M. Beck, L.W. Terstappen, Filtration parameters influencing circulating tumor cell enrichment from whole blood, PLoS. One 8 (4) (2013) e61774, https://doi.org/10.1371/journal.pone.0061774.

[34] S. Marcotti, G.C. Reilly, D. Lacroix, Effect of cell sample size in atomic force microscopy nanoindentation, J. Mech. Behav. Biomed. Mater. 94 (2019) 259–266, https://doi.org/10.1016/j.jmbbm.2019.03.018.

[35] J. Yang, P. Wang, Y. Zhang, M. Zhang, Q. Sun, H. Chen, L. Dong, Z. Chu, B. Xue, W. D. Hoff, C. Zhao, W. Wang, Q. Wei, Y. Cao, Photo-tunable hydrogels reveal cellular sensing of rapid rigidity changes through the accumulation of mechanical signaling molecules, Cell Stem Cell 32 (1) (2025) 121–136, https://doi.org/10.1016/j.stem.2024.09.016.

[36] A.N. Semenov, D.A. Gvozdev, A.M. Moysenovich, D.V. Zlenko, E.Y. Parshina, A. A. Baizhumanov, G.S. Budylin, E.G. Maksimov, Probing red blood cell membrane microviscosity using fluorescence anisotropy decay curves of the lipophilic dye PKH26, Int. J. Mol. Sci. 23 (24) (2022), https://doi.org/10.3390/ijms232415767.

[37] E. Evans, A. Yeung, Apparent viscosity and cortical tension of blood granulocytes determined by micropipet aspiration, Biophys. J. 56 (1) (1989) 151–160, https://doi.org/10.1016/S0006-3495(89)82660-8.

[38] M. Simon, M. Dokukin, V. Kalaparthi, E. Spedden, I. Sokolov, C. Staii, Load rate and temperature dependent mechanical properties of the cortical neuron and its pericellular layer measured by atomic force microscopy, Langmuir 32 (4) (2016) 1111–1119, https://doi.org/10.1021/acs.langmuir.5b04317.

[39] F.G. Strobl, F. Seitz, C. Westerhausen, A. Reller, A.A. Torrano, C. Bräuchle, A. Wixforth, M.F. Schneider, Intake of silica nanoparticles by giant lipid vesicles: influence of particle size and thermodynamic membrane state, Beilstein. J. Nanotechnol. 5 (1) (2014) 2468–2478, https://doi.org/10.3762/bjnano.5.256.

[40] G. Sagvolden, I. Giaever, E.O. Pettersen, J. Feder, Cell adhesion force microscopy, PNAS 96 (2) (1999) 471–476, https://doi.org/10.1073/pnas.96.2.471.
[41] M.J. Ueda, T. Ito, T.S. Okada, S.I. Ohnishi, A correlation between membrane fluidity and the critical temperature for cell adhesion, J. Cell. Biol. 71 (2) (1976) 670–674, https://doi.org/10.1083/jcb.71.2.670.
[42] D. Baier, T. Müller, T. Mohr, U. Windberger, Red blood cell stiffness and adhesion are species-specific properties strongly affected by temperature and medium changes in single cell force spectroscopy, Molecules 26 (9) (2021), https://doi.org/10.3390/molecules26092771.
[43] B. Cappella, W. Stark, Adhesion of amorphous polymers as a function of temperature probed with AFM force-distance curves, J. Colloid Interface Sci. 296 (2) (2006) 507–514, https://doi.org/10.1016/j.jcis.2005.09.043.
[44] M.E. Dokukin, N.V. Guz, I. Sokolov, Quantitative study of the elastic modulus of loosely attached cells in AFM indentation experiments, Biophys. J. 104 (10) (2013) 2123–2131, https://doi.org/10.1016/j.bpj.2013.04.019.
[45] G. Fläschner, C.I. Roman, N. Strohmeyer, D. Martinez-Martin, D.J. Müller, Rheology of rounded mammalian cells over continuous high-frequencies, Nat. Commun. 12 (1) (2021), https://doi.org/10.1038/s41467-021-23158-0.
[46] A.F. Sarioglu, N. Aceto, N. Kojic, M.C. Donaldson, M. Zeinali, B. Hamza, A. Engstrom, H. Zhu, T.K. Sundaresan, D.T. Miyamoto, X. Luo, A. Bardia, B. S. Wittner, S. Ramaswamy, T. Shioda, D.T. Ting, S.L. Stott, R. Kapur, S. Maheswaran, D.A. Haber, M. Toner, A microfluidic device for label-free, physical capture of circulating tumor cell clusters, Nat. Methods 12 (7) (2015) 685–691, https://doi.org/10.1038/nmeth.3404.
[47] R. Martinez Vazquez, G. Nava, M. Veglione, T. Yang, F. Bragheri, P. Minzioni, E. Bianchi, M. Di Tano, I. Chiodi, R. Osellame, C. Mondello, I. Cristiani, An optofluidic constriction chip for monitoring metastatic potential and drug response of cancer cells, Integr. Biol. 7 (4) (2015) 477–484, https://doi.org/10.1039/c5ib00023h.